Distributed acoustic sensing elastic least-squares reverse time migration

Ivan Lim Chen Ning & Paul Sava, Center for Wave Phenomena, Colorado School of Mines
Whitney Schultz & Jim Simmons, Reservoir Characterization Project, Colorado School of Mines

SUMMARY

Distributed acoustic sensing (DAS) acquisition in borehole environments has seen rapid growth recently. However, the majority of DAS imaging applications convert native strain observations to the equivalent displacement or velocity measurements in order to be compatible with conventional seismic data processing. In contrast, we formulate elastic least-square reverse time migration (ELSRTM) with the energy norm imaging condition for native DAS strain data. ELSRTM provides an accurate representation of the elastic subsurface through reduction of artifacts due to acquisition and inaccurate wavefield extrapolation. We validate the ELSRTM DAS formulation on a field dataset from the Eagle Ford shale formation. Our method not only attenuates artifacts caused by limitations of acquisition geometry and nonphysical wave modes, but also provides relative amplitudes of the subsurface reflectors that match the recorded data and enable reservoir characterization.

INTRODUCTION

Reverse time migration (RTM) relies on the simultaneous availability of the forward wavefield from the source and the backward wavefield from the receivers. An imaging condition, such as a zero-lag cross-correlation, combines both readily available source and receiver wavefields at all times and positions to generate the subsurface image. In elastic media, the imaging condition generally involves decomposing the wavefield into the respective P- and S-wave modes (Yan and Sava, 2008; Artman et al., 2009; Duan and Sava, 2015). Although P- and S-wave mode separation is possible in anisotropic media, the decomposition is computationally expensive and requires additional corrections for residual leakage (Yan and Sava, 2009, 2011, 2012; Cheng and Fomel, 2014).

In this paper, we adopt the energy norm imaging condition (Rocha et al., 2017) for least-squares imaging to generate a single scalar image and avoid the need for wave mode decomposition. In contrast with earlier publications, we adopt a different formulation for the energy operator that exploits the elastodynamics relation to avoid the need for additional partial derivatives. To accurately backward extrapolate the seismic observations at the receiver locations in the elastic media, both stress and displacement data are simultaneously required at the time of extrapolation (Gangi, 1970; Aki and Richards, 2002; Ravasi and Curtis, 2013; Wapenaar, 2014). Single or multicomponent displacement data only introduces nonphysical wave modes into the extrapolated elastic field, i.e., generate S-waves from recorded P-waves. These spurious wave modes contaminate the image and generate artifacts that degrade the final image. Acquisition of the full strain tensor through new multicomponent DAS systems (Lim Chen Ning and Sava, 2018a,b,c; Lim Chen Ning, 2019) can facilitate more accurate wavefield extrapolation that mitigate nonphysical wave modes.

Alternatively, least-square RTM is also capable of suppressing image artifacts that correspond to nonphysical wave modes, as this method aims to produce the subsurface model that best predicts the observed data. Least-squares methodology applied to elastic migrations includes RTM with imaging conditions following P- and S-wave decomposition (Ren et al., 2016; Duan et al., 2017; Feng and Schuster, 2017; Qu et al., 2017) or energy norm imaging condition (Rocha and Sava, 2018) where we adopt the latter approach. Moreover, we adopt the method known as prestack LSRTM when every single shot is treated as a separate inversion problem (Dai and Schuster, 2013; Huang et al., 2016; Liu et al., 2017; Agut et al., 2017) in order to mitigate the impact of inaccurate velocity on the image. Nevertheless, the accuracy of the subsurface structure still depends on the accuracy of the velocity model, but to a lesser degree as compared with methods that treats all shots in a single inversion.

In summary, we propose an ELSRTM method for DAS data using the energy norm which we formulate as a cascade linear operators. This formulation avoids the need for DAS data conversion to honor the native strain measurements, thus eliminating the inaccuracy associated with conversions.

METHODOLOGY

We describe forward elastic wavefield extrapolation using the second-order partial differential equations in space $\mathbf{x}$ and time t consisting of both stress $\underline{\mathbf{t}}(\mathbf{x},t)$ and particle displacement $\mathbf{u}(\mathbf{x},t)$ wavefields (Aki and Richards, 2002)

$$\rho\,\frac{\partial^2\mathbf{u}}{\partial t^2} = \mathbf{D}\,\underline{\mathbf{t}} + \mathbf{f}, \tag{1}$$

where $\rho(\mathbf{x})$ and $\mathbf{f}(\mathbf{x},t)$ are density and external volume force, respectively. The operator $\mathbf{D}$ denotes divergence. Under the assumption of linear elasticity the stress $\underline{\mathbf{t}}(\mathbf{x},t)$ is related to strain $\underline{\mathbf{e}}(\mathbf{x},t)$ through the constitutive relation

$$\underline{\mathbf{t}} = \underline{\underline{\mathbf{c}}}\,\underline{\mathbf{e}} + \underline{\mathbf{m}}, \tag{2}$$

where $\underline{\underline{\mathbf{c}}}(\mathbf{x})$ is the stiffness tensor and $\underline{\mathbf{m}}(\mathbf{x},t)$ is the seismic moment tensor source acting as stress perturbation. The relation between the strain $\underline{\mathbf{e}}(\mathbf{x},t)$ tensor and particle displacement $\mathbf{u}(\mathbf{x},t)$ is

$$\begin{aligned}\underline{\mathbf{e}} &= \frac{1}{2}\left\{\nabla\mathbf{u} + (\nabla\mathbf{u})^{\mathsf{T}}\right\}\\ &= \mathbf{H}\,\mathbf{u},\end{aligned} \tag{3}$$

where the operator $\mathbf{H}$ captures the geometric relation between strain and particle displacement. We solve equations 1 and 2 using the finite-difference representation of the time-derivative leading to the recursive relations for stress

$$\underline{\mathbf{t}} = \underline{\underline{\mathbf{c}}}\,\mathbf{H}\,\mathbf{u} + \underline{\mathbf{m}} \tag{4}$$

and particle displacement

$$\mathbf{u}_+ = 2\mathbf{u} + \frac{\Delta t^2}{\rho}\left(\mathbf{D}\underline{\mathbf{t}} + \mathbf{f}\right) - \mathbf{u}_- . \tag{5}$$

These recursive equations allow us to compute the subsequent time wavefield $\mathbf{u}_+$ from wavefields at the current time $\mathbf{u}$ and at preceding time $\mathbf{u}_-$. We express the forward operator $\mathbf{G}$ that takes an external force wavefield $\mathbf{p}(\mathbf{x},t) = [\underline{\mathbf{m}}(\mathbf{x},t), \mathbf{f}(\mathbf{x},t)]$ and generates the source wavefield $\mathbf{w}(\mathbf{x},t) = [\underline{\mathbf{t}}(\mathbf{x},t), \mathbf{u}(\mathbf{x},t)]$ by propagating forward in time:

$$\mathbf{w} = \mathbf{G}\mathbf{p} . \tag{6}$$

The adjoint operator $\mathbf{G}^\intercal$ takes the forward wavefield $\mathbf{w}(\mathbf{x},t) = [\underline{\mathbf{t}}(\mathbf{x},t), \mathbf{u}(\mathbf{x},t)]$ and generates the adjoint wavefield $\mathbf{p}(\mathbf{x},t) = [\underline{\mathbf{m}}(\mathbf{x},t), \mathbf{f}(\mathbf{x},t)]$ by propagating backward in time:

$$\mathbf{G}^\intercal\mathbf{w} = \mathbf{p} . \tag{7}$$

We solve for $\underline{\mathbf{m}}$ and $\mathbf{f}$ backward in time using the sources $\underline{\mathbf{t}}$ and $\mathbf{u}$. The time reversal iterative equation for the adjoint strain is

$$\underline{\mathbf{m}} = \mathbf{D}^\intercal\mathbf{f} + \underline{\mathbf{t}} \tag{8}$$

and the adjoint particle displacement is

$$\mathbf{f}_- = 2\mathbf{f} + \frac{\Delta t^2}{\rho}\left(\mathbf{H}^\intercal\underline{\underline{\mathbf{c}}}\,\underline{\mathbf{m}} + \mathbf{u}\right) - \mathbf{f}_+ . \tag{9}$$

We modify the potential term of the energy norm imaging condition from Rocha et al. (2017) to obtain the energy image $\mathcal{I}(\mathbf{x})$ which exploits the source wavefield (displacement and stress) $\mathbf{w}_s(\mathbf{x},t) = [\mathbf{u}_s(\mathbf{x},t), \underline{\mathbf{t}}_s(\mathbf{x},t)]$ together with the receiver wavefield (displacement and strain) $\mathbf{w}_r(\mathbf{x},t) = [\mathbf{u}_r(\mathbf{x},t), \underline{\mathbf{e}}_r(\mathbf{x},t)]$ as

$$\begin{aligned}
\mathcal{I}(\mathbf{x}) &= \sum_t \left(\rho\dot{\mathbf{u}}_s\cdot\dot{\mathbf{u}}_r - \underline{\mathbf{t}}_s\cdot\underline{\mathbf{e}}_r\right) \\
&= \left(\begin{bmatrix}\rho^{1/2}\mathbf{B} & 0\\ 0 & \mathbf{I}\end{bmatrix}\begin{bmatrix}\mathbf{u}_s & \underline{\mathbf{t}}_s\end{bmatrix}\right)^\intercal\begin{bmatrix}\rho^{1/2}\mathbf{B} & 0\\ 0 & \mathbf{I}\end{bmatrix}\begin{bmatrix}\mathbf{u}_r & -\underline{\mathbf{e}}_r\end{bmatrix} \\
&= (\square\mathbf{w}_s)^\intercal\,\square\mathbf{w}_r \\
&= (\square^\intercal\square\mathbf{w}_s)^\intercal\,\mathbf{w}_r \\
&= \mathbf{E}^\intercal\mathbf{w}_r ,
\end{aligned} \tag{10}$$

where $\square$ denotes the energy operator that captures the time derivative operator $\mathbf{B}$ and density parameter $\rho^{1/2}$. $\mathbf{E}^\intercal$ and $\mathbf{E}$ represent the energy norm migration and demigration operators. We express the receiver wavefields as a series of cascading operators

$$\mathbf{w}_r = \mathbf{G}^\intercal\mathbf{K}^\intercal\mathbf{d}_r , \tag{11}$$

where the adjoint operator $\mathbf{K}^\intercal$ injects the receiver data $\mathbf{d}_r$ at known locations for backward modeling by adjoint operator $\mathbf{G}$. We express the entire demigration process from the energy norm image $\mathcal{I}(\mathbf{x})$ to the receivers as

$$\begin{aligned}
\mathcal{I} &= \mathbf{E}^\intercal\mathbf{G}^\intercal\mathbf{K}^\intercal\mathbf{d}_r \\
&= \mathbf{L}^\intercal\mathbf{d}_r \\
\mathbf{L}\mathcal{I} &= \mathbf{d}_r .
\end{aligned} \tag{12}$$

The adjoint operator $\mathbf{L}^\intercal$ performs energy norm migration with the receiver data. To mimic the single component DAS strain measurements, we introduce a compliance operator $\mathbf{S}$ that converts the stress outputs to strain and a windowing operator $\mathbf{W}$ to restrict the output to a single component:

$$\mathbf{W}\mathbf{S}\mathbf{L}\mathcal{I} = \mathbf{d}_r . \tag{13}$$

The corresponding DAS migration (adjoint) operation is therefore

$$\mathbf{L}^\intercal\mathbf{S}^\intercal\mathbf{W}^\intercal\mathbf{d}_r = \mathcal{I} . \tag{14}$$

This formulation does not include an averaging operator that would capture the DAS gauge length, although its inclusion is not complicated (Lim Chen Ning and Sava, 2018a). An accurate averaging requires interpolation of the DAS receiver locations into a denser grid with subsequent decimation to its original positions. The effect of gauge length is important for optical fiber deployment with complex geometry due to non-unique directionality.

NUMERICAL EXAMPLE

We demonstrate our method on the model shown in Figure 1(a) together with the acquisition geometry (source in magenta and receivers in white). The background P- and S-wave velocity models are set to 2.0 km/s and 1.5 km/s, respectively. The energy norm RTM image for a single shot is shown in Figure 1(b), and depicts non-horizontal artifacts in the image. Correlation between physical and nonphysical wave modes gives rise to artifacts that affect the interpretability of the geological reflector. To reduce these artifacts, we apply 10 iterations of ELSRTM as shown in Figure 1(c). Least-squares imaging reduces the effects of the nonphysical wave modes that do not match the observed data.

FIELD DATA EXAMPLE

We validate our approach using a 2D line from a 3D DAS vertical seismic profile (VSP) survey acquired in Lavaca County, Texas, USA. The DAS data consist of two sections of the deviated well, the vertical and the horizontal portion respectively. DAS acquisition uses channel spacing of approximately 8 m with gauge length of 10 m. We use data from the vertical part of the borehole as we are unable to identify arrivals in the horizontal section due to the low signal-to-noise ratio and the directivity of DAS measurements. The left panel in Figure 2 shows the acquisition geometry together with the estimated P -wave velocity derived from first-break picking and the corresponding 1D profile. The graph in red represents the S-wave velocity calculated from the available well logs.

We remove the DAS interrogator noise by using 2D median filters. We also downsample the data from 1 to 2 ms with antialiasing. The DAS data in the vertical section of the well consist of upgoing and downgoing waves, with the former linked to primary reflections and the latter to direct arrivals and multiple reflections. We perform wavefield separation using an FK filter to attenuate the downgoing wavefields. Spiking deconvolution whitens the frequency spectrum together with a bandpass filter ($3-6-60-70$ Hz) to remove noise at high

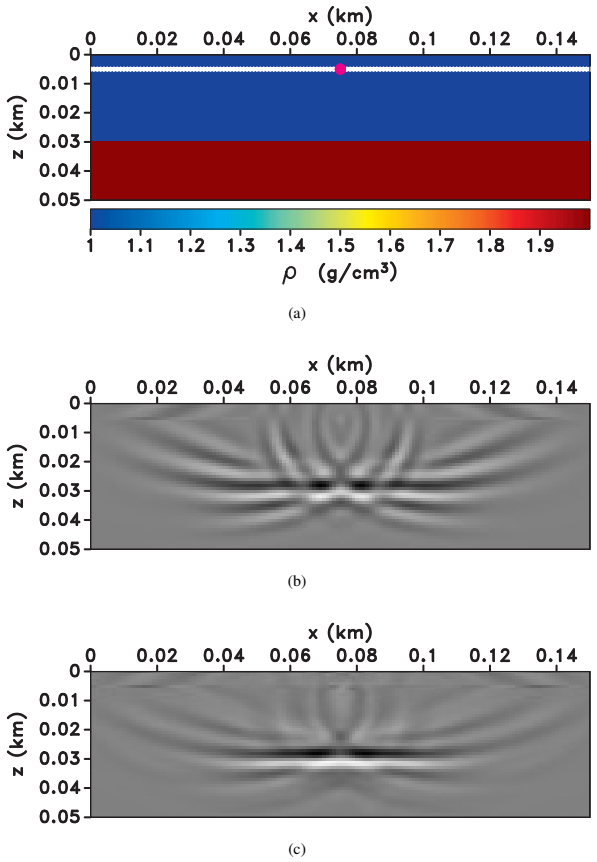

Figure 1: (a) Energy norm RTM image for a single shot (bottom right inset) and (b) the corresponding ELSRTM image after 10 iterations.

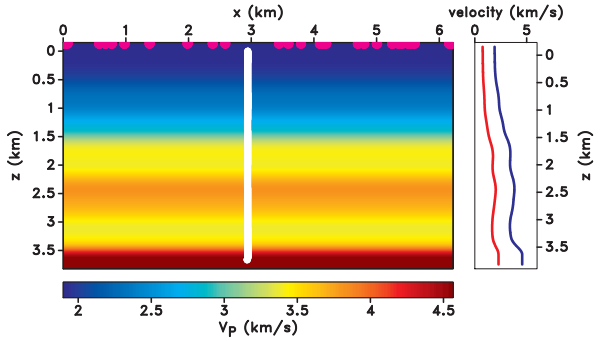

Figure 2: The left panel shows the P-wave velocity together with the acquisition geometry (sources in magenta and receivers in white). The blue and red graphs on the right panel represent the P- and S-wave velocity profiles, respectively.

frequencies. We apply additional denoising with 2D median filtering using flatten data and ray-tracing.

Figure 3(a) shows a single shot (location indicated at the bottom right) energy norm RTM image with the corresponding ELSRTM image in Figure 3(b). Figure 3(c) shows the initial residual for the single shot and Figure 3(d) is the final residual after 10 iterations of ELSRTM. In the final residual, we successfully fit the majority of the shallow reflectors above 1.5 km. Zoomed RTM and ELSRTM images are shown in Figures 4(a) and 4(b), respectively. The ELSRTM method attenuates reflectors that are due to the nonphysical S-waves, leading to higher resolution reflectors that present in the RTM image at $x = 3$ km and $z = 0.5$, 0.9, and 1.0 km.

We also perform ELSRTM for the remaining 35 shots and produce a final image by stacking. To improve the interpretability of the final image, we remove by dip filtering the steeply dipping migration smiles for every shot and apply automatic gain control (301 and 101 traces in depth and horizontal, respectively) in the final image to compensate for irregular source contributions. Shot regularization to a regular grid is necessary for even source contribution to improve the final stacking image quality. Figure 5(a) shows the DAS VSP image superimposed on the prestack time migration (PSTM) surface seismic image with time-to-depth conversion using the P-wave velocity in Figure 2 to demonstrate the continuity of reflectors between images. Although we note that the channel introduces lateral heterogeneity that present challenges for PSTM to accurately image the subsurface, the time migrated section is the only available image for referencing. The surface seismic image has undergo elaborate data processing and the migration velocity is different than the DAS VSP. Despite the lack of data regularization and the use of 1D velocity model, the DAS VSP image are able to match most of the reflectors within the vicinity of the borehole comparing with the surface seismic image. Figure 5(b) shows the equivalent surface seismic image without the overlay for direct comparison with the DAS VSP image. Note that the DAS VSP illumination increases with depth due to the acquisition geometry.

CONCLUSIONS

We propose elastic least-squares reverse time migration with the energy norm imaging condition for DAS data. The formulation honors the native DAS strain measurement without the need for conversion to displacement or velocity, thus avoiding the uncertainty and error associated with numerical implementations. Through the ELSRTM methodology, we suppress the imaging artifacts from nonphysical wave modes resulting from approximate backward wavefield extrapolation in the elastic media. The final ELSRTM images deliver geological reflectors that accurately predict the observed DAS data and minimize the data residuals. Additional pre-migration processing steps are necessary to optimize the final image including, shot amplitude balancing, shot regularization, and illumination compensation.

ACKNOWLEDGMENTS

We would like to thank the sponsors of the Center for Wave Phenomena and the Reservoir Characterization Program, whose support made this research possible. We are grateful to Devon Energy Corporation for permission to publish the Eagle Ford

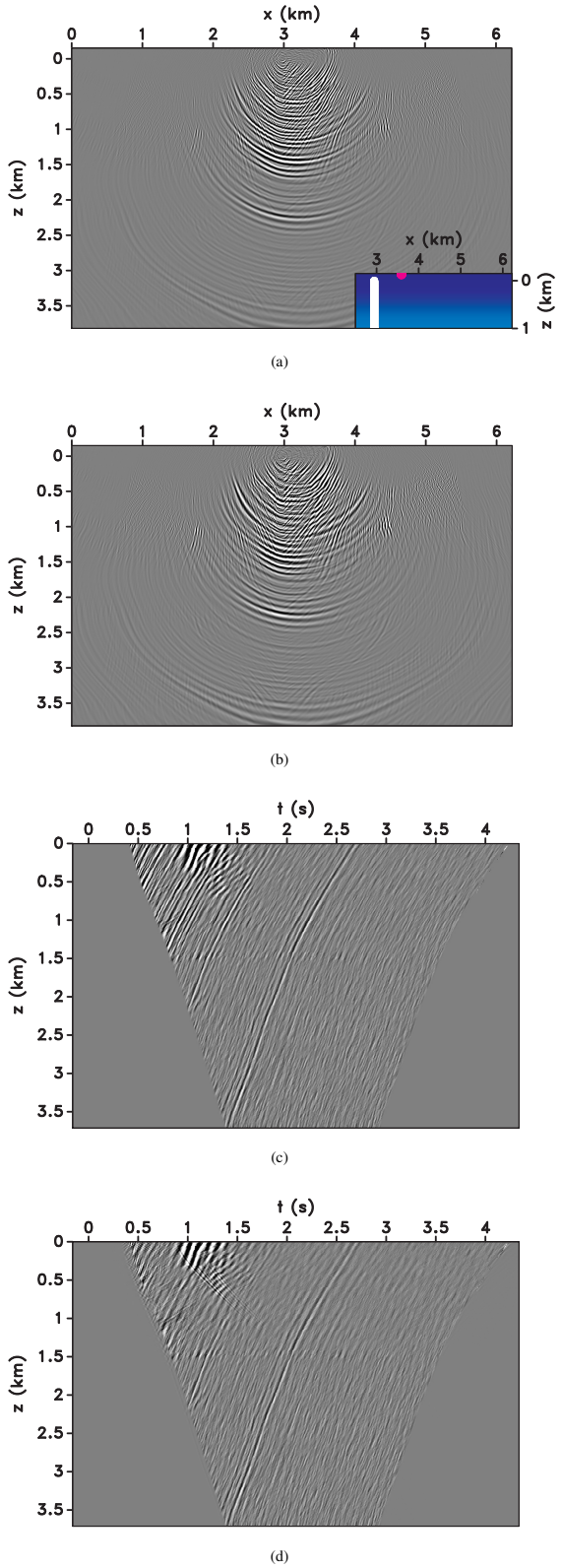

Figure 3: (a) Energy norm RTM image for a single shot (bottom right inset) and (b) the corresponding ELSRTM image after 10 iterations. (c) The initial data residual and (d) the final data residual after 10 iterations of ELSRTM.

Shale dataset. The reproducible numeric examples in this paper use the Madagascar open-source software package (Fomel et al., 2013) freely available from http://www.ahay.org.

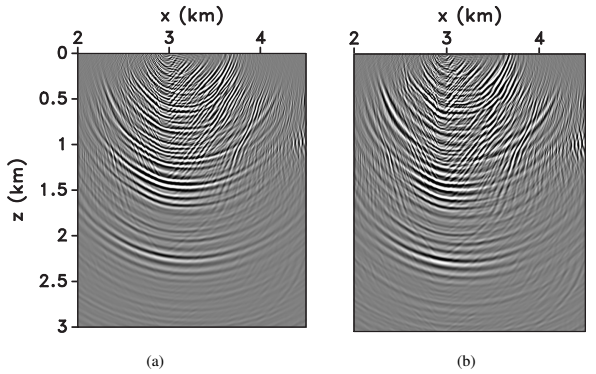

Figure 4: The zoom section of (a) the energy norm RTM image in Figure 3(a) and (b) the corresponding ELSRTM image in Figure 3(b).

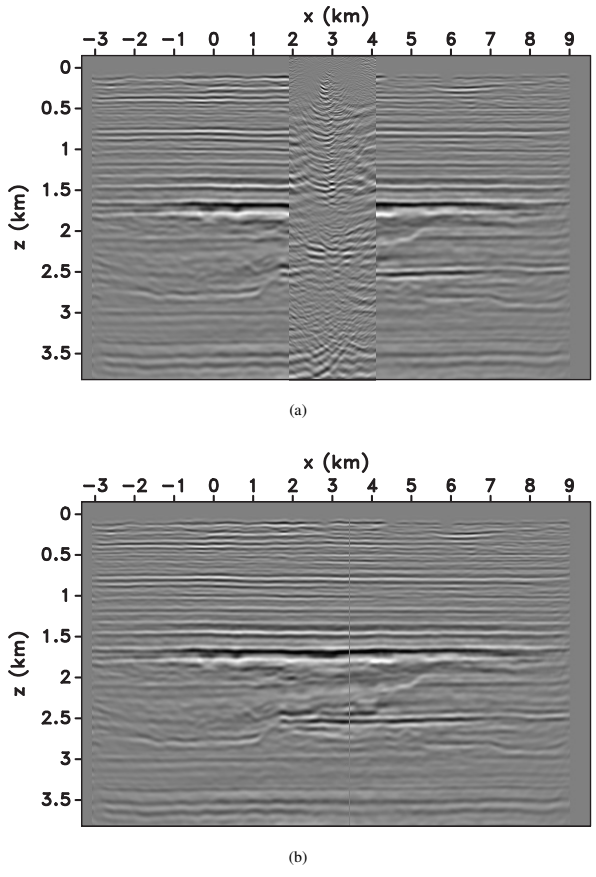

Figure 5: (a) ELSRTM DAS VSP image overlay the prestack time migration surface seismic image after time-to-depth conversion. (b) The corresponding surface seismic image without the overlay for direct comparison between DAS VSP.

REFERENCES

Agut, C., E. Bergounioux, V. Duprat, R. Baina, and P. Williamson, 2017, Prestack least-squares reverse time migration: Offset-domain regularization, *in* SEG Technical Program Expanded Abstracts 2017: Society of Exploration Geophysicists, 4524–4528.

Aki, K., and P. G. Richards, 2002, Quantitative seismology, 2 ed.: University Science Books.

Artman, B., I. Podladtchikov, and A. Goertz, 2009, Elastic time-reverse modeling imaging conditions, *in* SEG Technical Program Expanded Abstracts 2009: Society of Exploration Geophysicists, 1207–1211.

Cheng, J., and S. Fomel, 2014, Fast algorithms for elastic-wave-mode separation and vector decomposition using low-rank approximation for anisotropic media: Geophysics, **79**, C97–C110.

Dai, W., and G. T. Schuster, 2013, Plane-wave least-squares reverse-time migration: Geophysics, **78**, S165–S177.

Duan, Y., A. Guitton, and P. Sava, 2017, Elastic least-squares reverse time migration: Geophysics, **82**, S315–S325.

Duan, Y., and P. Sava, 2015, Scalar imaging condition for elastic reverse time migration: Geophysics, **80**, S127–S136.

Feng, Z., and G. T. Schuster, 2017, Elastic least-squares reverse time migration: Geophysics, **82**, S143–S157.

Fomel, S., P. Sava, I. Vlad, Y. Liu, and V. Bashkardin, 2013, Madagascar: open-source software project for multidimensional data analysis and reproducible computational experiments: Journal of Open Research Software, **1**.

Gangi, A. F., 1970, A derivation of the seismic representation theorem using seismic reciprocity: Journal of Geophysical Research, **75**, 2088–2095.

Huang, Y., R. Nammour, and W. Symes, 2016, Flexibly preconditioned extended least-squares migration in shot-record domain: Geophysics, **81**, S299–S315.

Lim Chen Ning, I., 2019, Multicomponent distributed acoustic sensing: Concept, theory, and applications: PhD thesis, Colorado School of Mines.

Lim Chen Ning, I., and P. Sava, 2018a, High-resolution multi-component distributed acoustic sensing: Geophysical Prospecting, **66**, 1111–1122.

———, 2018b, Multicomponent distributed acoustic sensing: Concept and theory: Geophysics, **83**, P1–P8.

———, 2018c, Multicomponent imaging with distributed acoustic sensing, *in* SEG Technical Program Expanded Abstracts 2018: Society of Exploration Geophysicists, 4683–4687.

Liu, X., Y. Liu, H. Lu, H. Hu, and M. Khan, 2017, Prestack correlative least-squares reverse time migration: Geophysics, **82**, S159–S172.

Qu, Y., J. Li, J. Huang, and Z. Li, 2017, Elastic least-squares reverse time migration with velocities and density perturbation: Geophysical Journal International, **212**, 1033–1056.

Ravasi, M., and A. Curtis, 2013, Elastic imaging with exact wavefield extrapolation for application to ocean-bottom 4C seismic data: Geophysics, **78**, S265–S284.

Ren, Z., Y. Liu, and M. K. Sen, 2016, Least-squares reverse time migration in elastic media: Geophysical Journal International, **208**, 1103–1125.

Rocha, D., and P. Sava, 2018, Elastic least-squares reverse time migration using the energy norm: Geophysics, **83**, S237–S248.

Rocha, D., N. Tanushev, and P. Sava, 2017, Anisotropic elastic wavefield imaging using the energy norm: Geophysics, **82**, S225–S234.

Wapenaar, C. P. A., 2014, Elastic wave field extrapolation: Redatuming of single-and multi-component seismic data: Elsevier, **2**.

Yan, J., and P. Sava, 2008, Isotropic angle-domain elastic reverse-time migration: Geophysics, **73**, S229–S239.

———, 2009, Elastic wave-mode separation for vti media: Geophysics, **74**, WB19–WB32.

———, 2011, Improving the efficiency of elastic wave-mode separation for heterogeneous tilted transverse isotropic media: Geophysics, **76**, T65–T78.

———, 2012, Elastic wave mode separation for tilted transverse isotropic media: Geophysical Prospecting, **60**, 29–48.